

ITO nanoparticles break optical transparency/high-areal capacitance trade-off for advanced aqueous supercapacitors

Sebastiano Bellani,^{a,†} Leyla Najafi,^{a,b,†} Gabriele Tullii,^{c,d} Alberto Ansaldo,^a Reinier Oropesa-Nuñez,^a Mirko Prato,^e Massimo Colombo,^f Maria Rosa Antognazza,^d and Francesco Bonaccorso^{*a}

^a *Graphene Labs, Istituto Italiano di Tecnologia, via Morego 30, 16163 Genova, Italy.*

^b *Università degli studi di Genova, Dipartimento di Chimica e Chimica Industriale, Via Dodecaneso 31, 16163 Genova, Italy.*

^c *Politecnico di Milano, Dip.to di Fisica, P.zza L. Da Vinci 32, 20133 Milano, Italy.*

^d *Center for Nano Science and Technology@Polimi, Istituto Italiano di Tecnologia, Via Pascoli 70/3, 20133 Milano, Italy.*

^e *Materials Characterization Facility, Istituto Italiano di Tecnologia, via Morego 30, 16163 Genova, Italy.*

^f *Nanochemistry, Istituto Italiano di Tecnologia, via Morego 30, 16163 Genova, Italy.*

† These authors contributed equally.

* Corresponding author: francesco.bonaccorso@iit.it

Experimental Section

Material and devices fabrication

Indium tin oxide nanoparticles (ITO NPs), ITO-coated glass slides (ITO FLAT) (area: $1 \times 1.5 \text{ cm}^2$, sheet resistance: $20 \text{ } \Omega \text{ } \square^{-1}$), ITO-coated PET (sheet resistance: $30 \text{ } \Omega \text{ } \square^{-1}$), rr-P3HT (electronic grade, M_n 15000-45000, 99.995% trace metals basis) and Na_2SO_4 (ACS reagent, $\geq 99.0\%$) are purchased from Sigma Aldrich. ITO FLAT and ITO-coated PET substrates are cleaned according to the following protocol: sequential sonication baths in deionized (DI) water, acetone (no for ITO-coated PET), isopropanol (IPA), each lasting for 10 min, and plasma cleaning in an inductively coupled reactor for 20 minutes (100 W RF power, excitation frequency 13.56 MHz, 40 Pa of O_2 gas process pressure, background gas pressure 0.2 Pa). 50 mg of ITO NPs are dispersed in 5 ml of ethanol (50 g L^{-1} concentration) by the aid of a probe sonicator (Branson digital sonifier) for 30 min at 10% power. ITO NPs dispersion is then drop-casted onto cleaned ITO FLAT substrates. Electrodes with ITO NPs mass loading of 0.125, 0.25, 0.5, 1.0 and 2.0 mg cm^{-2} are fabricated by varying the amount of the deposited ITO NPs dispersion. Electrode with ITO NPs mass loading of 1.0 mg cm^{-2} are also fabricated on 30 nm-thick Au substrate, as obtained by sputtering deposition on glass by a compact rotary-pumped coating system (Q150R, Quorum Technologies). The ITO NP electrodes are then annealed at $100 \text{ }^\circ\text{C}$ in order to remove solvent residuals. The rr-P3HT is dissolved in chlorobenzene at a concentration of 10 g L^{-1} . The dispersion is stirred at $50 \text{ }^\circ\text{C}$ for 12 h and then deposited by spin coating (1500 rpm) onto electrodes with an ITO NPs mass loading of 1 mg cm^{-2} . A thermal annealing treatment ($120 \text{ }^\circ\text{C}$ for 20 min, under N_2 atmosphere) completes the fabrication of the rr-P3HT-coated ITO NP electrodes.

Morphological, electrical and electrochemical characterization

X-ray photoelectron spectroscopy (XPS) is carried out with a Kratos Axis Ultra DLD spectrometer, using a monochromatic Al $\text{K}\alpha$ source (15 kV, 20 mA). The samples are prepared by drop-casting the as-prepared ITO NPs dispersion in ethanol onto 50 nm-Au sputtered coated silicon wafers. The samples are then dried under vacuum. The ITO FLAT is also measured as reference. High-resolution scans are performed at a constant pass energy of 10 eV and steps of 0.1 eV. The photoelectrons are detected at a take-off angle $\phi = 0^\circ$ with respect to the surface normal. The pressure in the analysis chamber is kept below 7×10^{-9} Torr for data acquisition. The binding energy scale is internally referenced to the Au $4f_{7/2}$ peak at 84 eV. The spectra are analysed using the CasaXPS software (version 2.3.16).

X-ray diffraction (XRD) is carried out by using PANalytical Empyrean with Cu K α radiation. The samples are prepared by drop-casting the as-prepared ITO NPs dispersion in ethanol onto a silicon wafer and dried under vacuum. The ITO FLAT is also measured as reference.

Transmission electron microscopy (TEM) images are taken by a JEM 1011 (JEOL) transmission electron microscope, operating at 100 kV. The as-prepared ITO NPs dispersion in ethanol is drop-casted onto carbon coated Cu TEM grids (300 mesh), rinsed with DI water and subsequently dried under vacuum overnight. Lateral dimensions of the ITO NPs are measured using ImageJ software (NIH). Statistical TEM analysis is carried out by means of OriginPro 9.1 software (OriginLab).

Atomic force microscopy (AFM) images are taken using a Nanowizard III (JPK Instruments, Germany) mounted onto an Axio Observer D1 (Carl Zeiss, Germany) inverted optical microscope. The AFM measurements are carried out by using PPP-NCHR cantilevers (Nanosensors, USA) with a nominal tip diameter of 10 nm. A drive frequency of \sim 295 kHz is used. Intermittent contact mode AFM images (512x512 data points) of $2.5 \times 2.5 \mu\text{m}^2$ and $500 \times 500 \text{nm}^2$ are collected keeping the working set point above 70% of the free oscillation amplitude. The scan rate for acquisition of the images is 0.7 Hz. Height profiles are processed by using the JPK Data Processing software (JPK Instruments, Germany) and the data are analysed with OriginPro 9.1 software (OriginLab). Statistical AFM analysis is carried out by means of OriginPro 9.1 software on four different AFM images. The samples are prepared by drop-casting the as-prepared ITO NPs dispersion in ethanol onto mica sheets (G250-1, Agar Scientific Ltd., Essex, U.K.).

UV-Vis absorption spectra of the ITO FLAT and ITO NPs electrode are collected using a Cary Varian 5000 UV-Vis spectrometer in transmission mode.

Specific surface area measurements are carried out by Kr physisorption at 77 K in Autosorb-iQ (Quantachrome). The specific surface areas are calculated using the multipoint Brunauer-Emmett-Teller (BET) model, considering 9 equally spaced points in the P/P_0 range from 0.10 to 0.30. P_0 is the vapour pressure of Kr at 77 K, corresponding to 2.63 Torr. Before the measurements, the samples are degassed for 1 h at 60 °C under vacuum conditions to eliminate weakly adsorbed species. The samples are ITO NPs powder and the ITO NP electrodes (ITO NPs mass loading of 0.25, 0.5, 1 and 2mg cm^{-2}) using ITO FLAT substrate.

Resistivity measurements are carried out by using a Hall effect analyser (Microworld, HMS5300), based on a four-probes van der Pauw method.¹ The measurements are carried out onto ITO NP films (mass loading of 0.5mg cm^{-2}) deposited directly on glass substrate (area of $1 \times 1 \text{cm}^2$) by

applying a 10 μA probing current and a mean magnetic field of 0.56 T. Indium contacts are fabricated at the edges of each sample to remove contact resistance between the ITO film and the Au probes.

Work function data of ITO FLAT and ITO NP films are obtained by using a Kelvin Probe (KP) system (KPSP020, KP Technologies Inc.). The measurements are carried out in air and at room temperature. Both a clean gold surface (WF = 4.8 eV) and a graphite sample (HOPG, highly ordered pyrolytic graphite, WF = 4.6 eV) are used as independent references for the probe potential.

Scanning electron microscope (SEM) analysis is performed with a field-emission scanning electron microscope FE-SEM (Jeol JSM-7500 FA). The acceleration voltage is set at 5kV. Images are collected using both below-the-lens secondary electron sensor (LEI images) and the in-lens secondary electron sensor (SEI images).

Electrochemical measurements on the as-prepared electrodes are carried out at room temperature in a flat-bottom fused silica cell under a three-electrode configuration using CompactStat potentiostat/galvanostat station (Ivium), controlled via Ivium's own IviumSoft. A Pt wire is used as the counter-electrode and saturated KCl Ag/AgCl is used as the reference electrode. Measurements are carried out in 200 mL 1 M Na_2SO_4 . Oxygen is purged from electrolyte by flowing N_2 gas throughout the liquid volume using a porous frit for 30 minutes before starting the measurements. Cyclic voltammetry (CV) measurements are performed in the voltage range between -0.2 and 1 V vs. Ag/AgCl at different scan rates (from 0.01 to 10 V s^{-1}). Charge discharge (CD) curves are acquired in the potential range between -0.2 and 1 vs. Ag/AgCl at different current densities (from 0.05 to 20 mA cm^{-2}). Electrochemical impedance spectroscopy (EIS) measurements are acquired in the 0.01 Hz \div 200 kHz frequency range at 0 V vs. Ag/AgCl with AC amplitude of 0.02 V.

Symmetric supercapacitors are tested in two-electrode configuration with CV and CD measurements in the aforementioned conditions. Transient voltage measurements are carried out to characterize the photo-charging property of the LP-S by measuring the open circuit voltage over time across the two electrodes after switching on/off simulated sunlight illumination (1.5AM illumination, 100 mW cm^{-2}).

Chemical, structural and morphological characterization of commercial ITO NPs

The chemical and structural composition of ITO NPs is studied by XPS (Fig. S1a-c) and XRD (Fig. S1d), respectively, and compared with that of commercial ITO-coated glass substrates (ITO FLAT). The XPS data (Fig. S1a-c) do not show significant differences between ITO NPs and ITO FLAT for the In 3d (Fig. S1a), Sn 3d (Fig. S1b) and O 1s spectra (Fig. S1c).² The percentage atomic content of In, Sn and O are 33.4%, 4.0% and 62.6%, respectively, for ITO FLAT, and 38.2%, 4.2% and 57.6%, respectively, for ITO NPs. The diffraction peaks in the XRD spectra (Fig. S1d) can be indexed to the body-centred cubic bixbyite In_2O_3 structure (PDF# 882160). No other components are here detected, suggesting that In atoms are effectively replaced by Sn atoms to form crystallized ITO NPs without formation of tin oxides, *e.g.*, SnO and SnO₂, which generate carrier traps at the grain boundaries to give lower carrier densities.^{3,4}

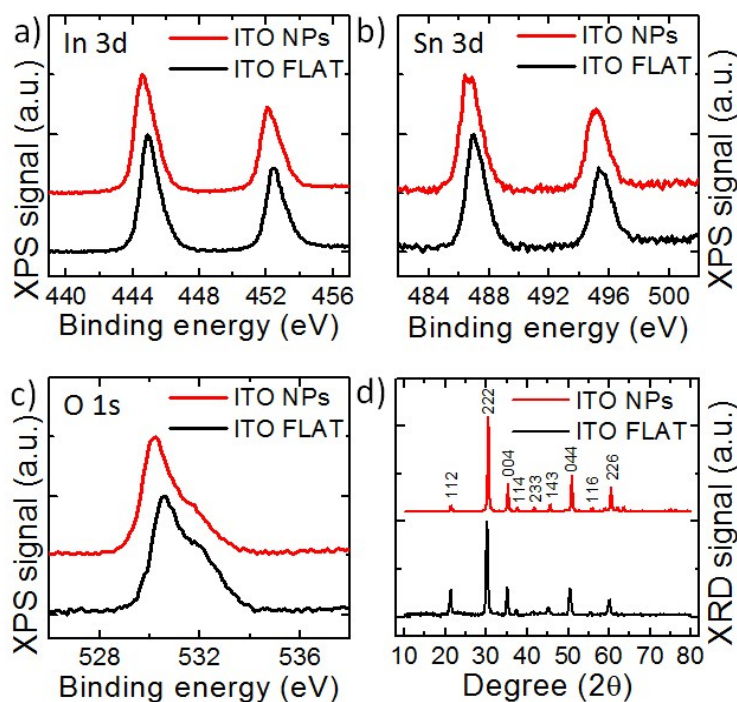


Fig. S1. XPS spectra of a) In 3d, b) Sn 3d and c) O 1s for ITO FLAT (black lines) and ITO NPs (red lines). d) XRD spectra for ITO FLAT and ITO NPs. The main diffraction peaks attributed to the body-centred cubic bixbyite In_2O_3 structure (PDF# 882160) are also indicated.

The morphology of ITO NPs is investigated by TEM (Fig. S2a-c) and AFM (Fig. S2d). TEM image of ITO NPs, drop casted onto carbon coated Cu TEM grids (Fig. S2a), clearly shows a cubic-like shape (in agreement with previous studies⁵ and the XRD measurements (Fig. S1d)) with lateral dimension < 50 nm (lognormal distribution peaking at 3.99 nm and a standard deviation of 0.89) (Fig. S2b). The TEM-selected area electron diffraction (TEM-SAED) of ITO NPs (Fig. S2c) gives sharp ring

pattern, indicating the polycrystalline nature of the samples, in agreement with XRD measurements (Fig. S1d). The AFM image of ITO NPs, drop casted onto mica (Fig. S2d), shows the presence of ITO NPs both as aggregates, on the left, and single, on the right. Height profiles of representative AFM image cross section indicates edge steps between 10 and 60 nm, in agreement with the lateral size of ITO NPs evidenced by TEM statistical analysis (Fig. S2b).

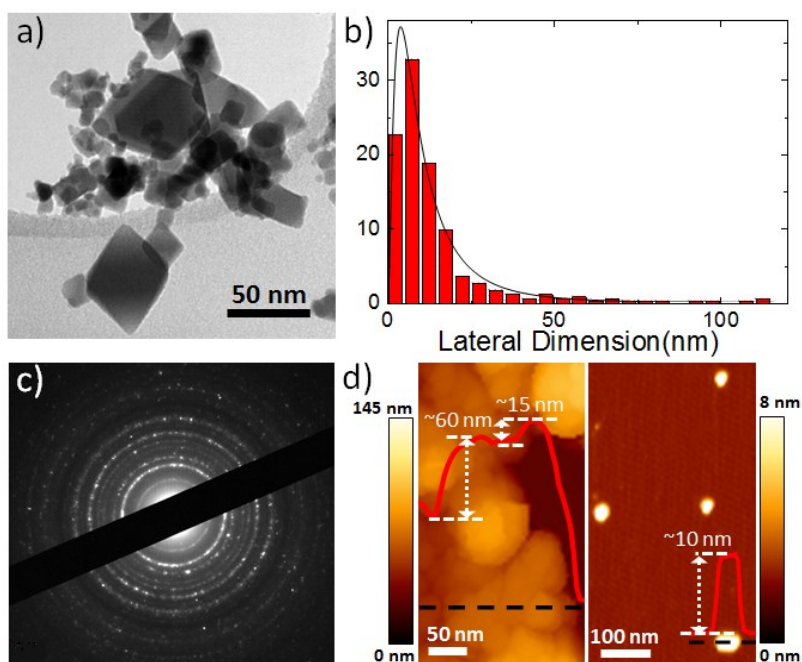


Fig. S2. a) TEM image of ITO NPs drop-casted onto carbon coated Cu TEM grids (300 mesh) from 0.1 mg mL^{-1} dispersions in ethanol. b) TEM statistical analysis of the lateral dimension of ITO NPs (derived from different images and calculated on 300 ITO NPs) c) TEM-SAED pattern of ITO NPs imaged in panel a). d) AFM images of ITO NP aggregates (left image) and single ITO NP (right image) deposited onto a V1-quality mica substrate from 0.1 mg mL^{-1} and 0.01 mg mL^{-1} . Height profiles of representative AFM image cross sections (dashed black lines) are also shown (red lines) evidencing the corresponding thickness (white dashed arrows).

SEM analysis of the electrodes with different ITO NPs mass loading

In the main text, Figs 2a-d show the top-view SEM images of electrode with ITO NPs mass loading of 0.5 mg cm^{-2} . The images reveal the mesoporous structure of the electrode, demonstrating a complete ITO NPs coverage of the ITO FLAT substrate. The same SEM analysis is also performed on the electrode with different ITO NPs mass loading (0.125 , 0.25 , 1 and 2 mg cm^{-2}) (**Fig. S3**). The corresponding images do not show remarkable differences.

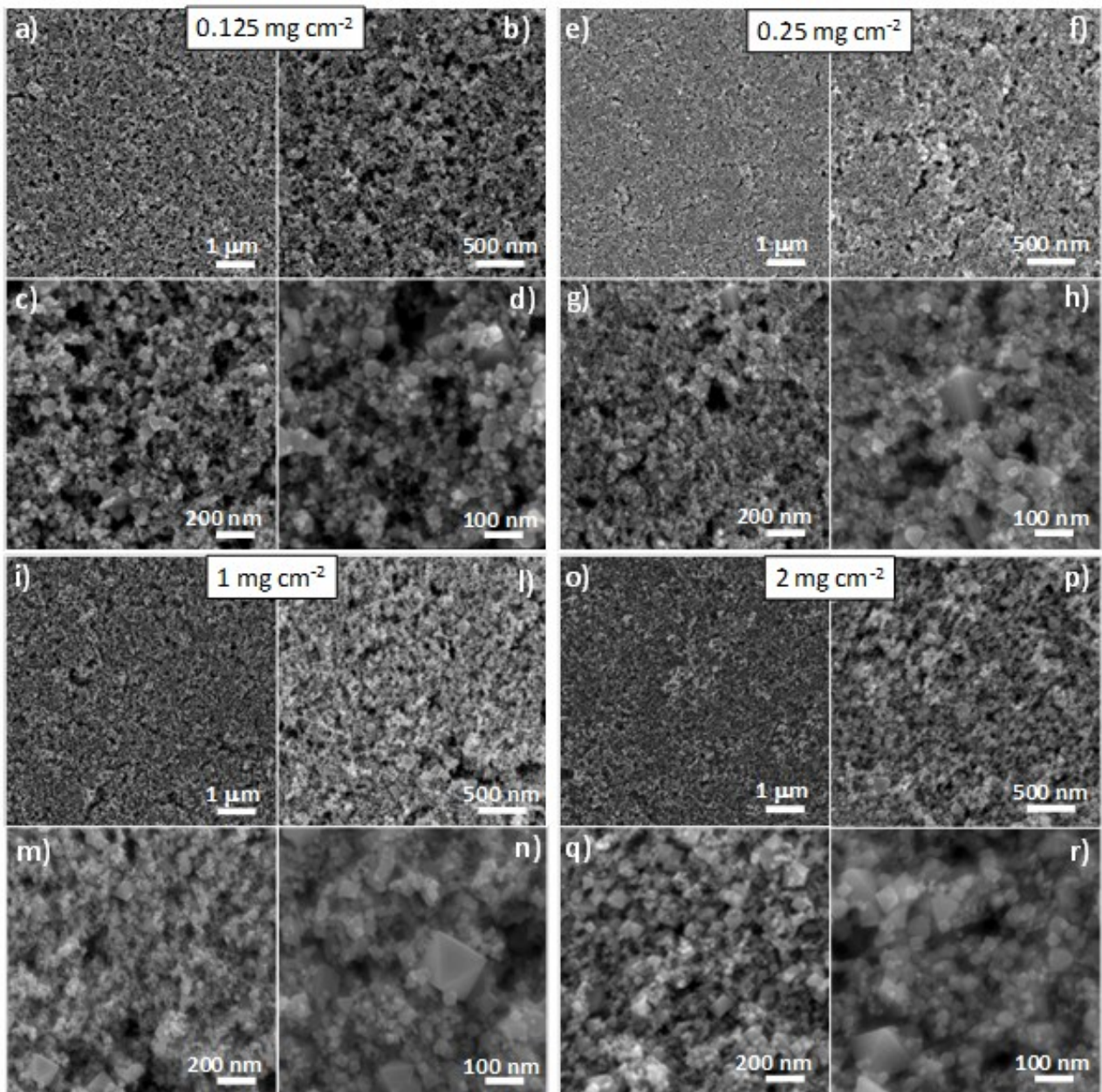


Fig. S3. Top-view SEM images of electrodes with ITO NPs mass loading of a-d) 0.125 mg cm^{-2} , e-h) 0.25 mg cm^{-2} , i-n) 1 mg cm^{-2} and o-r) 2 mg cm^{-2} at increasing magnifications.

However, at lower magnification ($120 \times 120 \mu\text{m}^2$ area) ITO NP aggregates are observed in the electrode with ITO NPs mass loading of 2 mg cm^{-2} (**Fig. S4**). Consequently, cracking-like effects of

the 2 mg cm⁻² ITO NPs film cause a partial coverage of the underlying ITO FLAT substrate. It is worth to note, however, that the electrochemical performance of the electrode with ITO NPs mass loading of 2 mg cm⁻² is not significantly affected by the anomalous morphology. In fact, this electrode shows the highest electrode current density (up to 6 mA cm⁻² at 1 V s⁻¹) in CV measurements (Fig. 3a) and the highest electrode C_{areal} values (e.g., 3.17 mF cm⁻² at 10 mA cm⁻²) (Fig. 3e), as calculated from CD curves (Fig.s 3c).

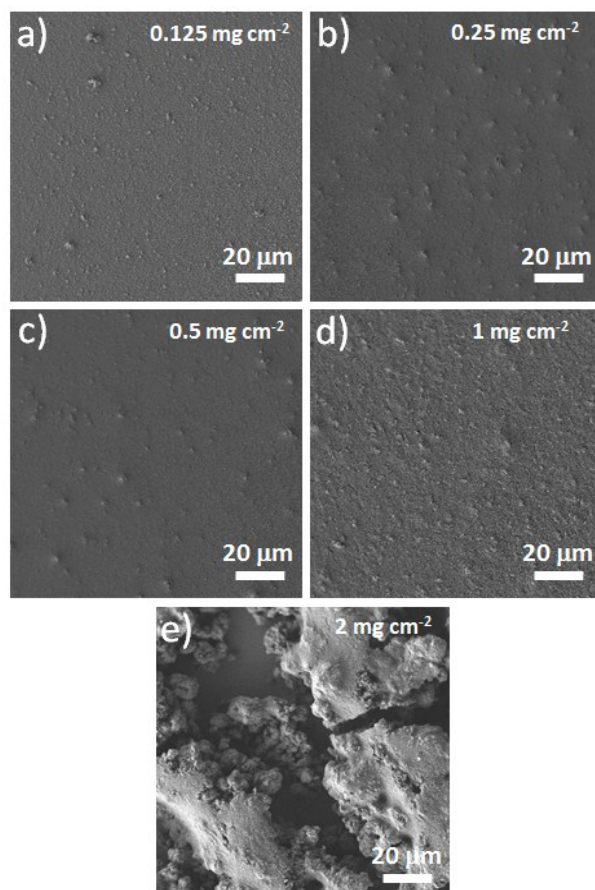


Fig. S4. Top-view SEM images of electrodes with ITO NPs mass loading of a) 0.125 mg cm⁻², b) 0.25 mg cm⁻², c) 0.5 mg cm⁻², d) 1 mg cm⁻² and e) 2 mg cm⁻² at low magnification (120×120 μm² area).

Identification of the capacitive potential range of ITO FLAT electrode

Fig. S5 reports the CV curve for the ITO FLAT electrode between -0.4 and 1.2 V vs. Ag/AgCl at a scan rate of 0.2 V s^{-1} . These data clearly show the presence of both irreversible reduction reaction, below -0.2 V vs Ag/AgCl, and oxidation reaction above 1 V vs. Ag/AgCl. In order to avoid non-capacitive currents, the potential range between -0.2 and 1 V vs. Ag/AgCl is selected for the CV and CD characterizations of the ITO-based electrode (see Fig. 3 in the main text).

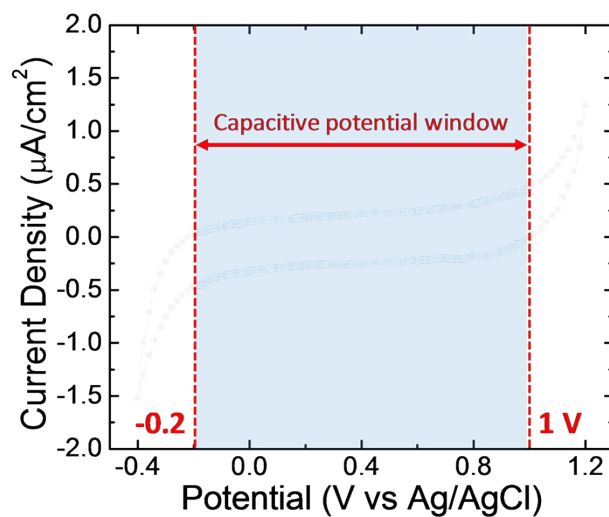


Fig. S5. CV curve for the ITO FLAT electrode at a scan rate of 0.2 V s^{-1} .

Cyclic voltammetry analysis of the electrode with different ITO NPs mass loading

Fig. S6 reports the CV curves at different scan rates (from 0.01 to 10 V s^{-1}) obtained for the electrodes with different ITO NPs mass loading (0.125, 0.5, 1 and 2 mg cm^{-2}), complementing the data reported in the main text for the electrode with ITO NPs mass loading of 0.25 mg cm^{-2} (Fig. 3b). These results evidence that the CV shapes become increasingly biconvex (lens-shaped) only at scan rate higher than 5 V s^{-1} for the highest ITO NP mass loadings (*i.e.*, 1 and 2 mg cm^{-2}). In these experimental conditions, current densities above 5 mA cm^{-2} are observed and only a fraction of capacitive states hold on with the applied voltage due to the losses ascribed to the equivalent series resistance (ESR) of the electrodes ($\sim 27 \Omega$, see **Fig. S9**).

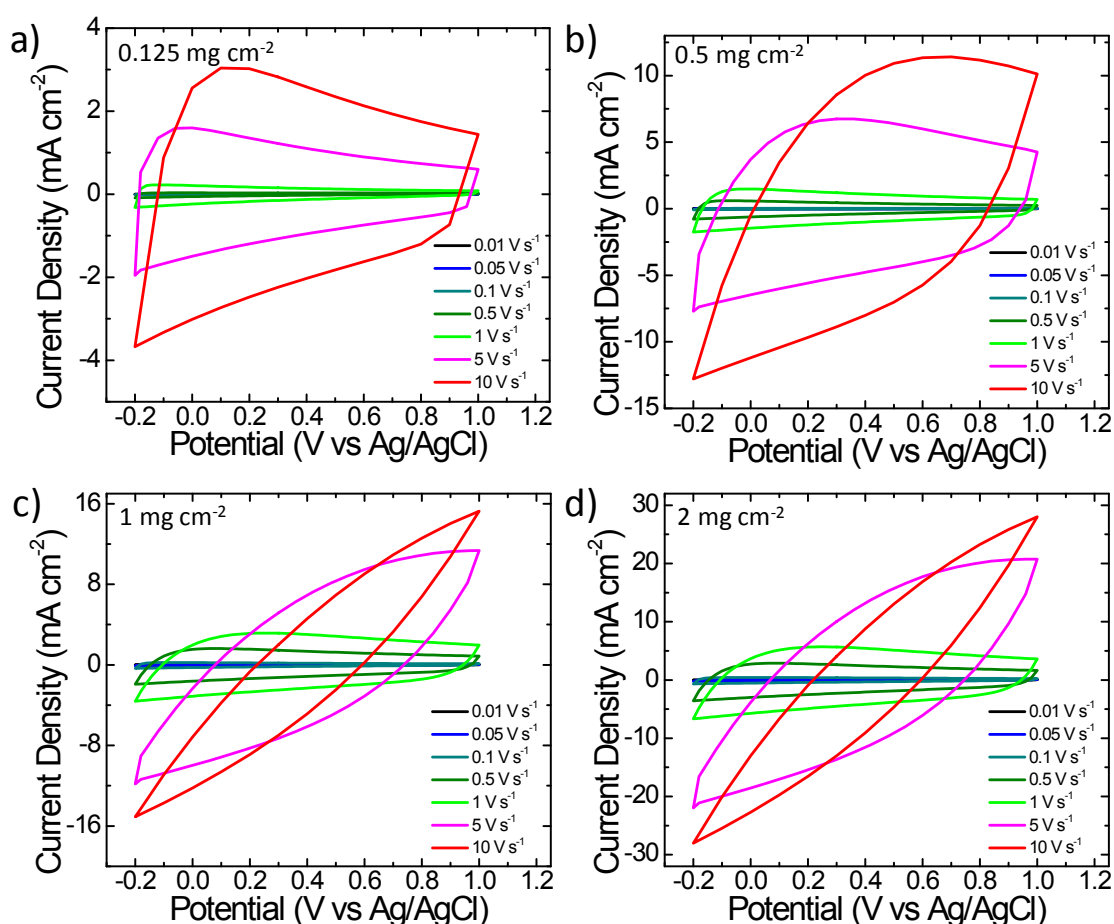


Fig. S6. The CV curves for the electrodes with ITO NPs mass loading of a) 0.125, b) 0.5, c) 1 and d) 2 mg cm^{-2} at different scan rate (from 0.01 V to 10 V s^{-1}).

Charge-discharge curves of the electrode with different ITO NPs mass loading

Fig. S7 shows the CD curves at different current densities (from 0.05 to 10 mA cm⁻²) obtained for the electrodes with different ITO NPs mass loading (0.125, 0.5, 1.0 and 2.0 mg cm⁻²), complementing the data reported in the main text for the electrode with ITO NPs mass loading of 0.25 mg cm⁻² (Fig. 4d).

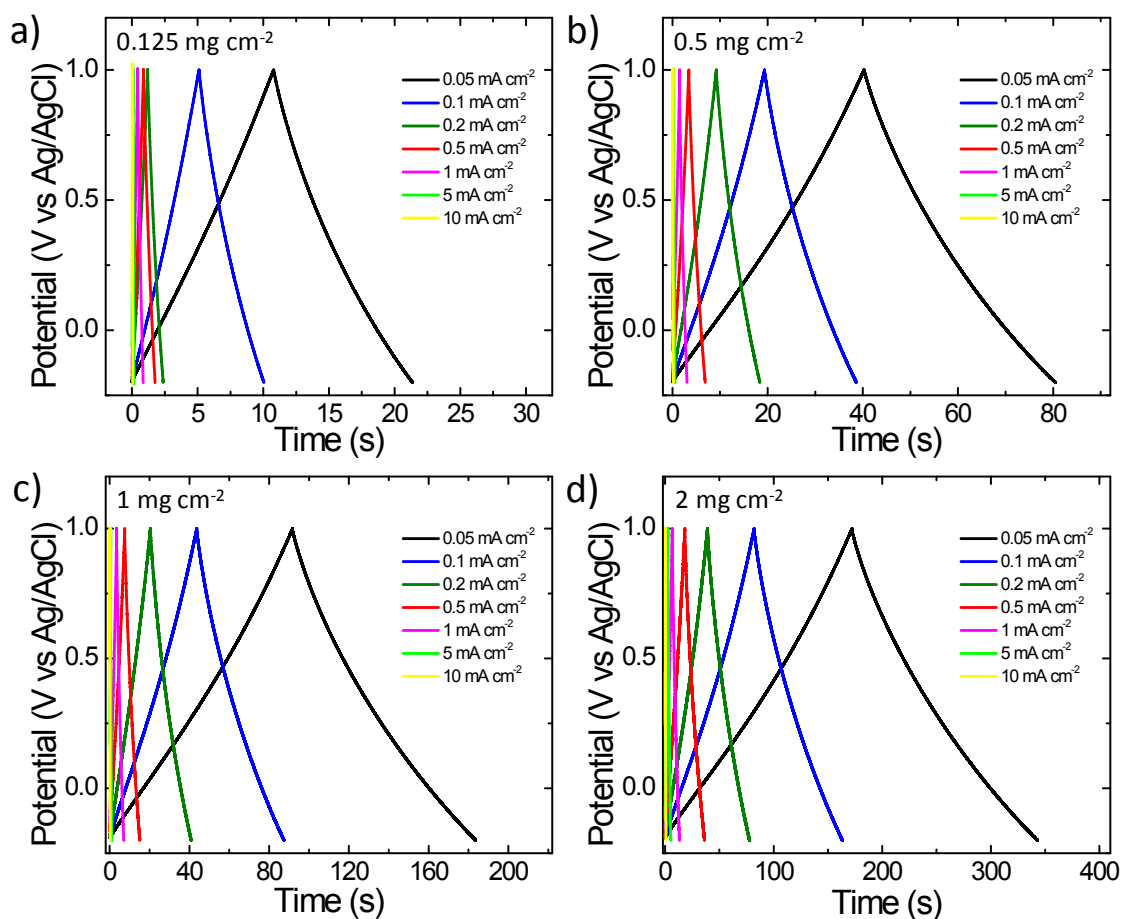


Fig. S7. The CD curves for the electrodes with ITO NPs mass loading of a) 0.125, b) 0.5, c) 1.0 and d) 2.0 mg cm⁻² at different current densities (from 0.05 to 10 mA cm⁻²).

Cycling stability of ITO NP electrodes

Fig. S8 reports 10000 CD cycles at current density of 1 mA cm^{-2} obtained for a representative electrode (ITO NPs mass loading of 0.25 mg cm^{-2}). The shape and the charging/discharging time are not significantly affected over the different cycles. As shown in the main text (Fig. 3e), capacitance retention of 99%, 97% and 94% over 100, 1000 and 10000 cycles, respectively, indicates the absence of mechanical breakdown. Moreover, the coulombic efficiency of $\sim 100\%$ for each cycle (Fig. 3e) means that the capacitive performance is not limited by parasitic chemical reactions.

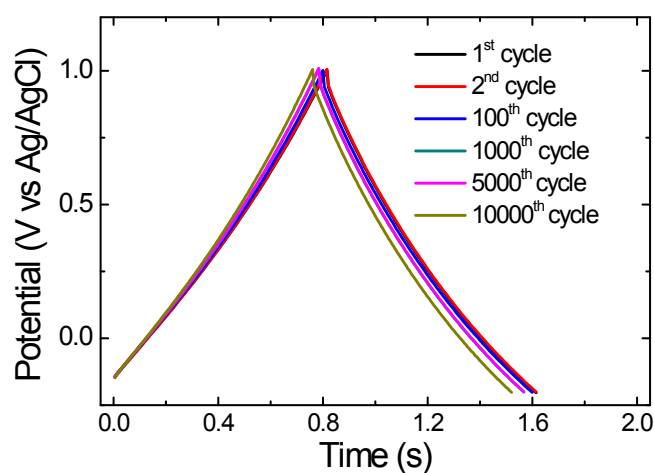


Fig. S8. Comparison of the galvanostatic CD curves at 1 mA cm^{-2} for 1st, 2nd, 100th, 1000th, 5000th and 10000th cycle for a representative electrode with ITO NPs mass loading of 0.25 mg cm^{-2} .

Equivalent series resistance of the ITO NP electrodes with ITO FLAT and Au substrates

Fig. S9a shows the galvanostatic CD curves at 10 and 20 mA cm⁻² for representative electrodes with ITO NPs mass loading of 1 mg cm⁻² using ITO FLAT and 30 nm thick Au substrate. **Fig. S9b** reports the dependence of the C_{areal} on the charging/discharging current densities (from 1 to 50 mA cm⁻²) for the same devices. The ESR values of the electrode using ITO FLAT substrate, as calculated by CD curves at 10 mA cm⁻², is 27±3 Ω. This value is comparable to the sheet resistance ($20 \pm 2 \Omega \square^{-1}$) of the ITO FLAT substrate, thus suggesting that the electrode ESR is limited by the resistance of the ITO FLAT substrate. Similar conclusion is also derived by EIS measurements. **Fig. S10a,b** report the bode plots of the electrochemical impedance (Z) (*i.e.*, the module of Z ($\text{mod}(Z)$) vs. frequency, and the $-\text{phase}(Z)$ vs. frequency) of the ITO FLAT and ITO NP electrodes with different mass loading (ranging from 0.125 to 2.0 mg cm⁻²). **Figure S10c,d** show the parameter R_s and C_s extracted by simplifying the equivalent circuit of the electrode/electrolyte systems (*i.e.*, the supercapacitor electrodes) with frequency (f)-dependent RC circuit, as illustrated in **Fig. S10e**. The detailed description of the equivalent circuit used for representing the supercapacitor electrodes and the corresponding simplified RC circuit have been reported in previous works (see Refs. 54, 66-70 of the main text). Briefly, at high frequency (frequency > 1 kHz) R_s approximates ESR of the supercapacitor electrode, while at low f ($f < 100$ Hz) C_s is comparable to the capacitance of the supercapacitor electrode. The results clearly evidence that the R_s of ITO NP electrodes at high f is independent by the mass loading, resembling that of ITO FLAT. These results are in agreement with the previous ESR analysis derived from the CD curves. *Vice versa*, the C_s of ITO FLAT and ITO NP electrodes at low f increases with the ITO NP mass loading, providing similar values to that obtained with ITO FLAT and ITO NP electrode capacitances extrapolated from the analysis of the CD curves in the main text (**Fig. 3c**). As commented in the main text, the use of more conductive transparent substrates could, in principle, permit to extend the capacitive activity of the electrodes at higher current density (> 10 mA cm⁻²). In fact, the analysis of the CD curve for the Au substrate-based electrode (sheet resistance of $4 \pm 1 \Omega \square^{-1}$) gives an ESR value of ~5 Ω. This enables to achieve C_{areal} of 2.37 (1.65) mF cm⁻² at 20 (50) mA cm⁻², *i.e.*, enhancing the C_{areal} of the electrode fabricated onto ITO FLAT substrate (1.02 (0.54) mF cm⁻²) of 132% (205%) (**Fig. S9b**).

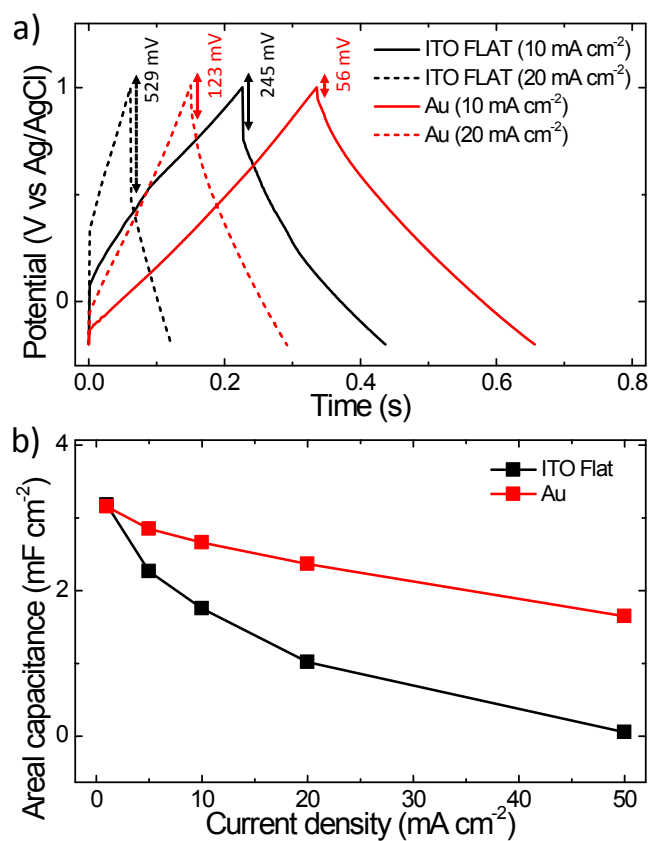


Fig. S9. a) Comparison of the CV curves of electrodes with ITO NPs mass loading of 1 mg cm⁻² deposited onto ITO FLAT (black lines) and Au (red lines) substrates at current densities of 10 mA cm⁻² (solid lines) and 20 mA cm⁻². The voltage drop at half cycle, used for ESR estimation, is indicated for each curve. b) Dependence of the C_{areal} on the charging/discharging current densities (from 1 to 50 mA cm⁻²) for the same devices of panel a). Solid lines are a guide to the eye.

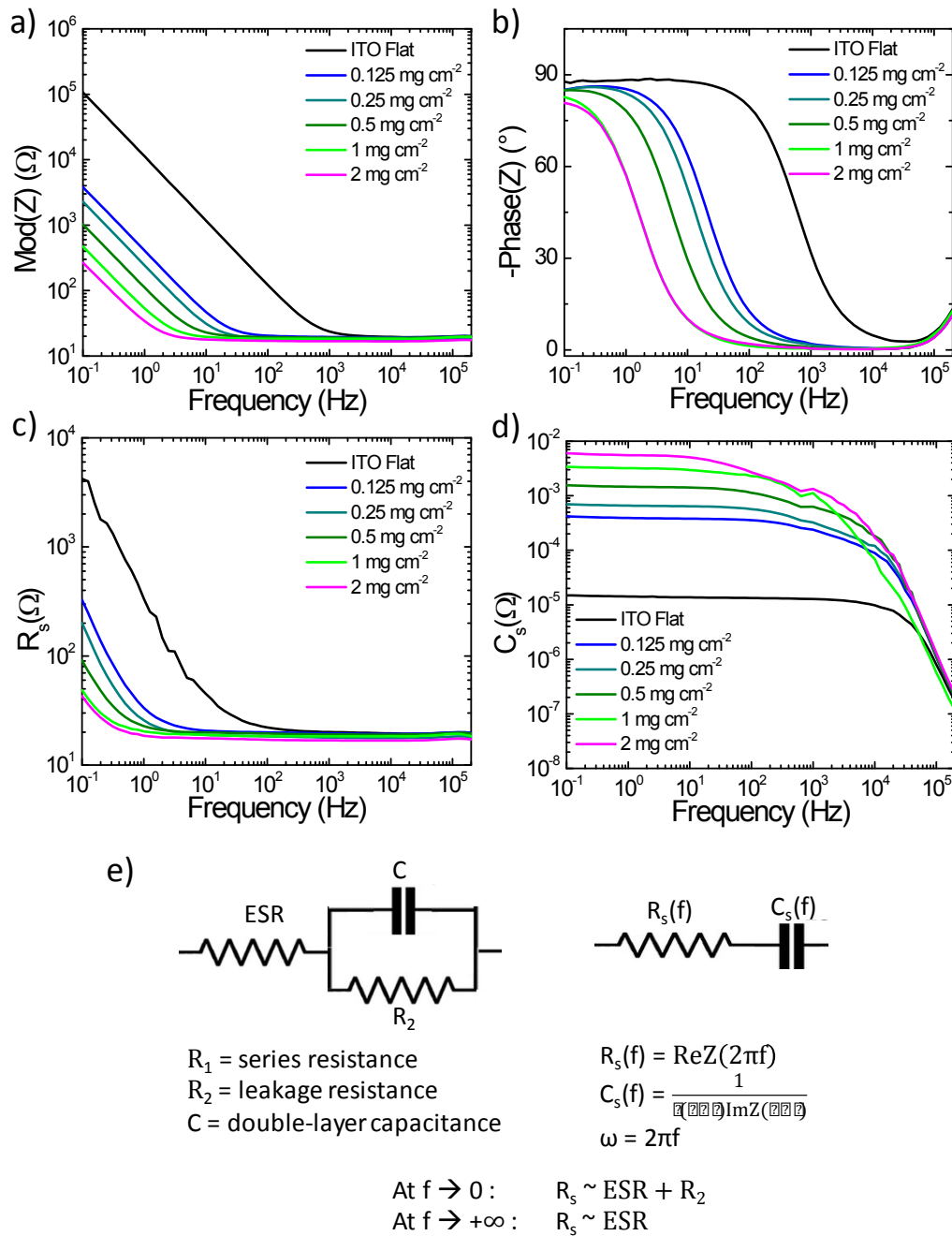


Fig. S10. a,b) Bode plots of the module (panel a) and the phase (panel b) of the electrochemical impedance (Z) (*i.e.*, $\text{mod}(Z)$ and $-\text{phase}(Z)$, respectively) of the ITO FLAT and ITO NP electrodes with different mass loading (from 0.125 to 2 mg cm⁻²). c,d) Frequency dependence of the electrical parameters R_s and C_s of the RC circuits simplifying the equivalent circuit of the supercapacitor ITO FLAT and ITO NP electrodes with different mass loading (from 0.125 to 2 mg cm⁻²). e) On the left: equivalent electrical circuit of the electrode/electrolyte systems (*i.e.*, supercapacitor electrodes), expressed by the series of the ESR and a parallel RC circuit given by leakage resistance (R_2) and the double-layer capacitance (C); on the right: frequency (f)-dependent RC circuit, given by the series between $R_s(f)$ and $C_s(f)$, which simplifies the equivalent circuit of the supercapacitor electrodes. At low f , *i.e.*, $f \rightarrow 0$, $R_s \sim \text{ESR} + R_2$; at high f , *i.e.*, $f \rightarrow \infty$, $R_s \sim \text{ESR} + R_2$. Electrical modelling details of the electrodes are reported in Refs. 54,66-77 of the main text).

Fig. S11 reports all the CD curves measured at different current densities (from 1 to 50 mA cm⁻²) for the Au substrate-based ITO NPs electrode.

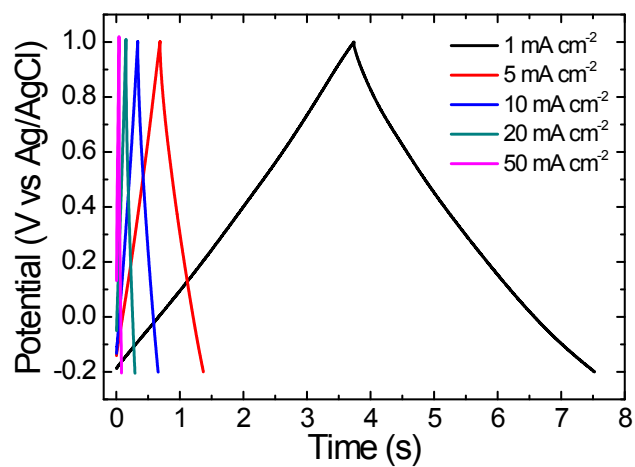


Fig. S11. CD curves at different current densities (from 1 to 10 mA cm⁻²) of the electrode with ITO NPs mass loading of 1 mg cm⁻², deposited onto Au substrate.

Flexible ITO NPs electrode

As reported in the main text, flexible ITO NP electrodes are fabricated onto ITO-coated polyethylene terephthalate (PET) substrates. **Fig. S12a** shows a photograph of a representative flexible electrode with ITO NPs mass loading of 1.0 mg cm^{-2} . Fig. S12b shows the electrode capacitance retention at current density of 1 mA cm^{-2} over 100 bending cycles at curvature radius (R) of 1.0 and 0.5 cm. For $R = 1.0 \text{ cm}$, the capacitance increases of 25.4% with respect to the initial values ($\sim 2.96 \text{ mF cm}^{-2}$) after the first bending cycles, and it progressively stabilizes after 100 bending cycles ($C_{\text{areal}} = 3.94 \text{ mF cm}^{-2}$). The increase of the capacitance with the first bending cycles could be attributed to a mesoscopic rearrangement of the ITO NPs with respect to the as-produced electrode. For $R = 0.5 \text{ cm}$, the capacitance decreases mainly during the first bending cycles, retaining 67.8% of its initial value after 100 bending cycles.

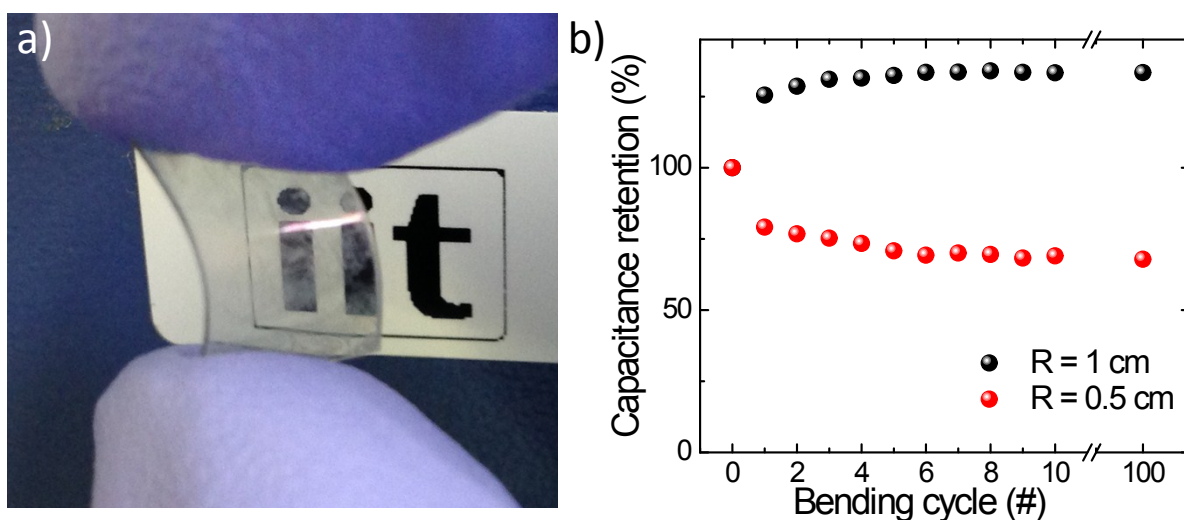


Fig. S12. a) Photograph of a representative flexible electrode with ITO NPs mass loading of 1 mg cm^{-2} on ITO-PET substrate. b) Capacitance retention at current density of 1 mA cm^{-2} of the flexible electrode with ITO NPs mass loading of 1 mg cm^{-2} over 100 bending cycles with radius of curvature (R) of 1 cm (black spheres) and 0.5 cm (red spheres).

Areal capacitance of the symmetric ITO NP supercapacitors

The C_{areal} values calculated from CD curves for the symmetric supercapacitor (single electrode ITO NPs mass loading of 1 mg cm^{-2}) is reported in **Fig. S13**, in comparison with those obtained for the corresponding single electrodes. The decrease of the C_{areal} with the applied current density is ascribed to the ESR-related capacitive losses, as for the cases of the single electrodes. The ESR value for the symmetric supercapacitor, as estimated from the CD curves analysis, is $60 \pm 5 \Omega$. This value is given by the sum of the sheet resistances of the ITO FLAT substrates and the electrolyte resistance. As reported in the main text, the C_{areal} values at current density lower than 1 mA cm^{-2} (where ESR-related capacitive losses are limited) are ~ 2 times lower with respect to those of the single electrodes with ITO NPs mass loading of 1 mg cm^{-2} , being the C_{areal} of the symmetric supercapacitor the series of those of the two single electrodes.

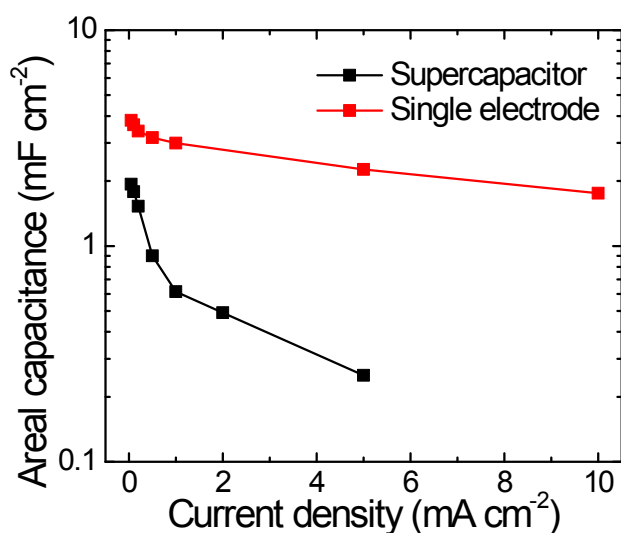


Fig. S13. Comparison of the C_{areal} obtained for the supercapacitor and the corresponding single electrodes with ITO NPs mass loading of 1.0 mg cm^{-2} .

Transmittance spectra of ITO NPs electrode before and after rr-P3HT infiltration

Fig. S14 shows the transmittance (T) spectra of the ITO NPs electrode (ITO NPs mass loading of 1.0 mg cm^{-2}) before and after rr-P3HT infiltration (rr-P3HT deposited by following the protocol described in Experimental section, Material and devices fabrication). Clearly, after rr-P3HT infiltration, the electrode shows a decrease of the T in the 350-700 nm wavelength range, as expected from rr-P3HT absorption spectra (band peaking at $\sim 520 \text{ nm}$, with other features at $\sim 550 \text{ nm}$, $\sim 610 \text{ nm}$ and $\sim 660 \text{ nm}$).⁶

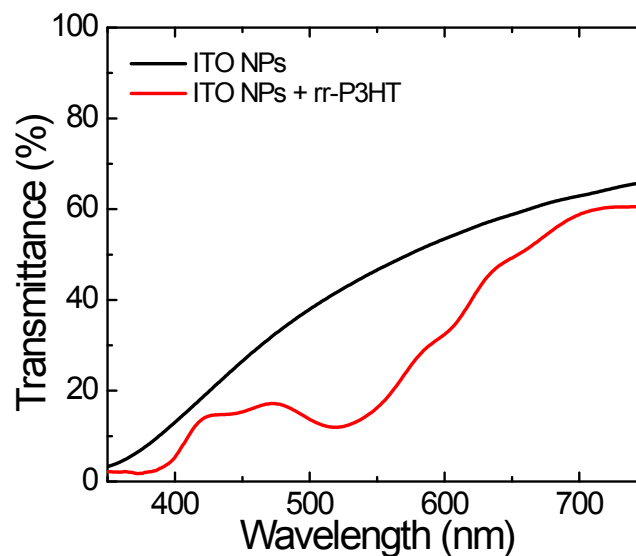


Fig. S14. Transmittance spectra of the ITO NP electrodes with different ITO NPs mass loading of 1 mg cm^{-2} on 100 nm thick ITO FLAT substrate a) before (ITO NPs, black line) and b) after rr-P3HT infiltration (ITO NPs + rr-P3HT, red line).

References

- 1 L. J. van der Pauw, *Philips Res. Repts.* 1958, **13**, 1.
- 2 V. M. Bermudez, A. D. Berry, H. Kim, A. Pique, *Langmuir* 2006, **22**, 11113.
- 3 R. B. H. Tahar, T. Ban, Y. Ohya, Y. Takahashi, *J. Appl. Phys.*, 1998, **83**, 2139.
- 4 G. Frank, H. Kostlin, *Appl. Phys. A: Mater. Sci. Process* 1982, **27**, 197.
- 5 Y. Yang, D. Du, F. Kong, J. Fan, T. Qiu, *J. Appl. Phys.* 2015, **117**, 245307.
- 6 S. Bellani, D. Fazzi, P. Bruno, E. Giussani, E. V. Canesi, G. Lanzani, M. R. Antognazza, *J. Phys. Chem. C* 2014, **118**, 6291.